ISIJ International, Vol. 32 (1992), No. 1, pp. 66–75

Behaviour of Bubbles at Gas Blowing into Liquid Wood's Metal

Yongkun XIE, Stefan ORSTEN and Franz OETERS

Institute for Metallurgy, Berlin Technical University, Strasse des 17 Juni 135, 1000 Berlin 12, Germany.

(Received on July 23, 1991; accepted in final form on September 20, 1991)

Experimental studies on the bubble behaviour in submerged gas blowing were carried out with liquid Wood's metal. About 440 kg of Wood's metal at 100°C was contained in a ladle-shaped glass vessel with an inner diameter of 40 cm. The liquid metal was stirred by nitrogen, argon or helium respectively through a nozzle positioned centrically or eccentrically at the bottom. The bubble plumes were investigated under different gas flow rates and nozzle diameters by determination of local gas fraction, bubble frequency, size distribution and rising velocity of bubbles.

The measurements show that the radial distribution of gas fraction and bubble frequency can be described by a Gaussian function and the bubble size distribution obeys a log-normal function. Except for the region near the nozzle the mean rising velocity of bubbles is nearly constant over the radius. The influence of blowing conditions on these variables was estimated.

KEY WORDS: ladle metallurgy; gas stirring; bubble behaviour; Wood's metal; electroresistivity probe.

1. Introduction

In the steel industry the endeavours for better utilization of energy and of raw materials with simultaneous improvement of product quality have lead to the development of the procedures of secondary metallurgy, partly also called ladle metallurgy. Within the secondary metallurgy the gas stirring treatment with Ar or N_2 in ladle is an important procedure.

In order to be able to describe and control the metallurgical processes in the ladle, knowledges about the behaviour of gas bubbles, *e.g.* the size and the duration of bubbles in metal bath, are necessary. Because of the high operating temperatures direct measurements in the steel melt are difficult. Hence one has been increasingly endeavoured in recent years to perform measurements at model systems.[1-8] Usually water was used as modelling liquid. In comparison with liquid steel the physical properties of water however are quite different. Therefore our understanding of the phenomena mentioned might be improved by direct measurements at a liquid metal.

In this paper experimental studies on the bubble behaviour in molten Wood's metal were carried out. By use of double-contact electroresistivity probes the local gas fraction, the bubble frequency, the size distribution and the rising velocity of bubbles were measured under different blowing conditions.

2. Experimental Procedure

2.1. Modelling Liquid

In the present paper a low-melting-point alloy called "Wood's metal" was used as modelling liquid. It consists of 50%bismuth–25%lead–12.5%tin–12.5%cadmium and has a melting point of 70°C. As to be seen in **Table 1**, the density and the viscosities of the Wood's metal lie essentially closer to the values of the liquid iron than those of water and mercury. The surface tension of the Wood's metal is indeed lower than that of iron, however it is much higher than that of water.

2.2. Experimental Apparatus

Figure 1 shows the schematic representation of the experimental apparatus. As model vessel serves a temperature resistant glass vessel with an inner diameter of 40 cm and a height of 1 m. The vessel is placed on a bottom plate of 2 cm thick stainless steel plate. The

Table 1. Comparison of physical properties of liquid iron and various modelling liquids.

Liquid	Density (g/cm^3)	Surface tension (g/sec^2)	Kinematic viscosity (cm^2/sec, 10^{-2})	Dynamic viscosity ($g/cm \cdot sec$, 10^{-2})
Iron	7.0	1 680–1 850	0.629–0.886	4.4–6.2
Water	1.0	73	1.0	1.0
Mercury	13.6	465	0.114	1.55
Wood's metal[9]	9.4	460	0.447	4.2

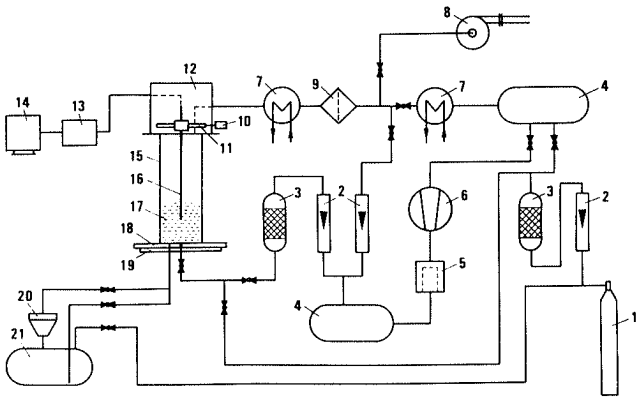

1. Gas cylinder
2. Flow meters
3. Copper catalyser
4. Pressure tanks
5. Oil filter
6. Compressor
7. Coolers
8. Ventilator
9. Gas filter
10. Stepping motor
11. Traverser
12. Top cover
13. Electronics
14. Computer
15. Glass vessel (I.D. 40 cm)
16. Measuring lance
17. Wood's metal
18. Stainless steel plate
19. Heating (7.5 kW)
20. Ceramic filter
21. Stainless steel vessel

Fig. 1. Schematic diagram of the experimental apparatus with Wood's metal as modelling liquid.

bottom plate is electrically heated by a flat heating with a capacity of 7.5 kW. In the bottom plate there are one centrically and several eccentrically positioned hole-type nozzles. In the cover which locks up the model vessel at the top a two-dimensional traverser is integrated. It serves for the attachment of the measuring lance and its positioning in radial and vertical direction.

In order to reduce the gas consumption and to avoid Wood's metal emissions, a closed gas loop system has been constructed. The inert gas which leaves the model vessel after having been injected into the melt is lead to a compressor and after compression anew blown through the nozzles into the melt. Beforehand the gas is lead through a copper catalyser in order to remove oxygene traces from it. Via a low-pressure regulating valve the system is continuously being admitted fresh inert gas which has been lead through another copper catalyser cartridge before. It serves for the compensation of the losses of gas which result from the leakiness of the system.

Before starting an experiment the Wood's metal is heated up and molten in a steel vessel by electrical rod heaters. After the metal in the vessel has reached a temperature of about 100°C, an overpressure in the vessel is set up by nitrogen and the melt is pressed through a heated pipe into the model vessel. For the accomplished experiments the model vessel was filled with 46.5 *l* which is about 440 kg of Wood's metal up to a bath height of 37 cm.

2.3. Measuring Devices

Double-contact electroresistivity probes were used for the measurements. **Figure 2** shows the construction of a probe applied in this paper. It consists of two fine steel capillary tubes with an outer diameter of 0.45 mm and

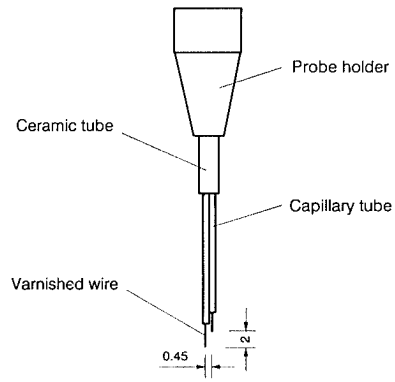

Fig. 2. Schematic diagram of a double-contact electroresistivity probe.

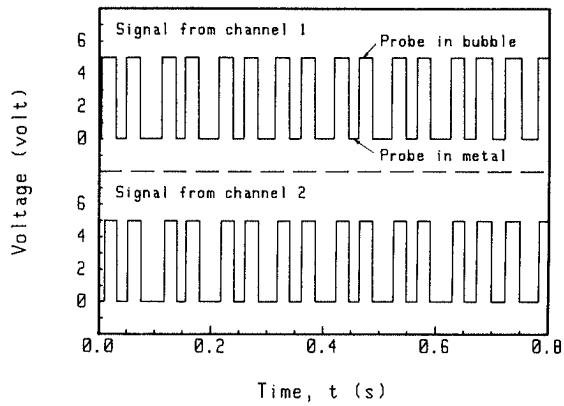

Fig. 3. Signals obtained from a double-contact electroresistivity probe in Wood's metal.

an inner diameter of 0.25 mm. These serve as mechanical protection of the electrodes which consist of a varnished copper wire with a diameter of 0.2 mm and except for the peak are electrically isolated. The vertical shifting of the two electrodes amounts to 2 mm.

The measuring principle of the double-contact electroresistivity probes is known from earlier papers.[2,4,5] The exactitude of the measurement with double-contact electroresistivity probes primarily depends on the quality of the voltage signals. It is all the higher the shorter the times of ascent and descent of the voltage pulses are. **Figure 3** reproduces the signal pattern recorded by a 2-channel-storage oscilloscope in the molten Wood's metal. The change between the upper and lower voltage level generally takes place within three and five microseconds which are at least three orders of magnitude shorter than the duration of the single pulse itself which lies in the range of 2 to 80 ms. With a such ideal signal pattern the exactitude of the measurement is guaranteed.

For the performance of the measurements two devices were used for the data acquisition. A 2-channel-digital-storage oscilloscope was employed for the measurement of the local gas fraction and the bubble frequency. A counter, in which ten single meter units are integrated, served for the measurement of the rising velocity and the pierce length of bubbles. The data measured by the devices are registered, evaluated and storaged by a respective computer.

2.4. Blowing Conditions and Measuring Arrangements

The experiments were carried out in two series with centric and eccentric nozzle position. For the centric gas blowing the local gas fraction, the bubble frequency, the rising velocity and the pierce length of bubbles were investigated for six different gas flow rates of 100, 200, 300, 500, 800 and 1 200 Ncm^3/sec (Ncm^3/sec *i.e.* cm^3/sec at standard temperature and pressure). In order to determine the influence of the nozzle diameter, nozzles with an inner diameter of 2, 3 and 5 mm were employed. In consideration of the axial symmetry for centric blowing the measurements were carried out on a vertical plane going through the center of the vessel. The measuring points were placed at a level of 5 up to 35 cm above the nozzle. The axial distance between the measuring points amounted to 5 cm. Because of the bubble plume broadening to the top the measurements were taken through in different radius ranges becoming larger to the top.

Due to the stochastic character of the bubble plume it is by all means necessary for fused results to carry out a plurality of single measurements. The duration for measurements of the gas fraction and the bubble frequency amounted for each measuring point to about 5 min. For measurements of the rising velocity and the pierce length of bubbles the measuring time depended on the local bubble density. At each point 1 000 bubbles were measured.

In case of eccentric blowing the nozzle was placed at a distance of half of the vessel radius off the wall. With this position the gas distribution for four gas flow rates, namely 100, 200, 500 and 800 Ncm^3/sec with a nozzle diameter of 3 mm was investigated.

Most of all the measurements were carried out by blowing with nitrogen, in some cases argon or helium was used. The temperature of the molten metal in the model vessel remained at 100°C.

3. Results

3.1. Distribution of Gas Fraction

In order to determine the area of the interface between gas bubbles and molten metal, the gas volume in the molten metal should be known. For this purpose the spatial distribution of the gas fraction was measured. **Figure 4** represents as an example the radial distributions of gas fraction measured in case of centric blowing with a gas flow rate of 200 Ncm^3/sec and at various planes above the nozzle. By means of a regression analysis the statement of earlier papers can be confirmed that the radial distribution of the local gas fraction obeys a Gaussian function. Thus the relation

$$\Phi = \Phi_m \exp(-r^2/b_\Phi^2) \quad \text{.....(1)}$$

applies to the dependence of the local gas fraction on the radial position. Φ_m is the axial gas fraction and the exponential factor b_Φ describes the width of the bubble plume which is characterized as such that the ratio Φ/Φ_m will be equal to $1/e$ if $r = b_\Phi$.

The results of the measurements have shown that

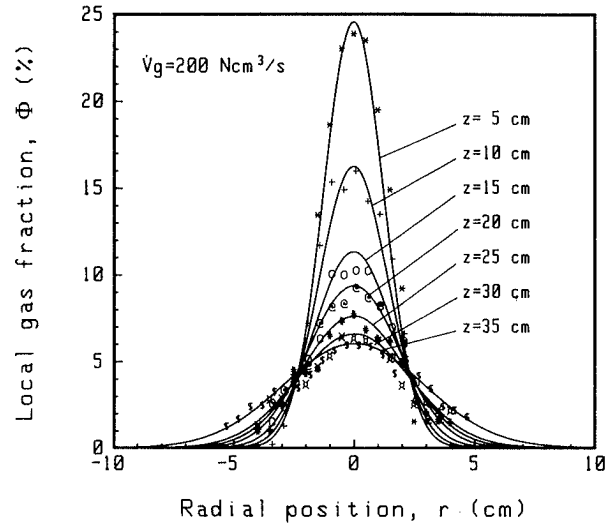

Fig. 4. Profiles of gas fraction at various heights.

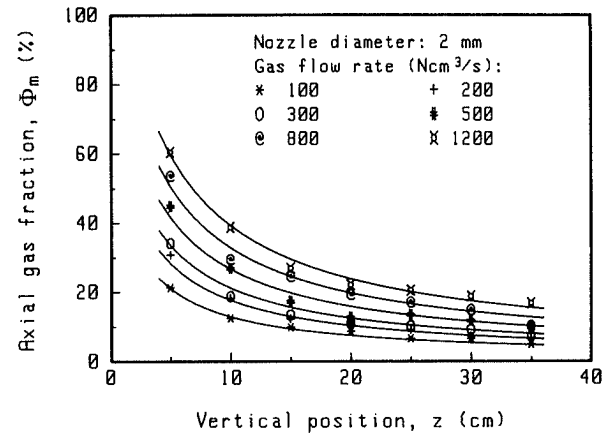

Fig. 5. Axial gas fraction as a function of height for various gas flow rates.

both parameters Φ_m and b_Φ substantially depend on the gas flow rate and on the distance above the nozzle. In **Fig. 5** the measured axial gas fractions for various gas flow rates and a nozzle diameter of 2 mm are presented. The value of Φ_m reduces with increasing distance from the nozzle and becomes larger with growing gas flow rate.

From the accomplished measurements the following relation was found:

$$\Phi_m \propto \dot{V}_{g,z}^{1/2}/(z + H_o) \,. \quad \text{.....(2)}$$

$\dot{V}_{g,z}$ represents the gas flow rate corresponding to the pressure and temperature in the melt at height z. It is expressed by

$$\dot{V}_{g,z} = \dot{V}_{g,N} T_l p_N / T_N [p_N + g\rho_l (H - z)] \,. \quad \text{.....(3)}$$

H_o is the distance between the nozzle and the mathematical origin of the plume.[10] The value of H_o first of all depends on the nozzle diameter and the gas flow rate. Within the performed measuring range the following equation resulted:

$$H_o = 4.5 d_o^{1/2} (\dot{V}_{g,o}^2/g)^{1/10} \,, \quad \text{.....(4)}$$

where d_o represents the nozzle diameter and $\dot{V}_{g,o}$ the gas flow rate at the nozzle position. By means of a

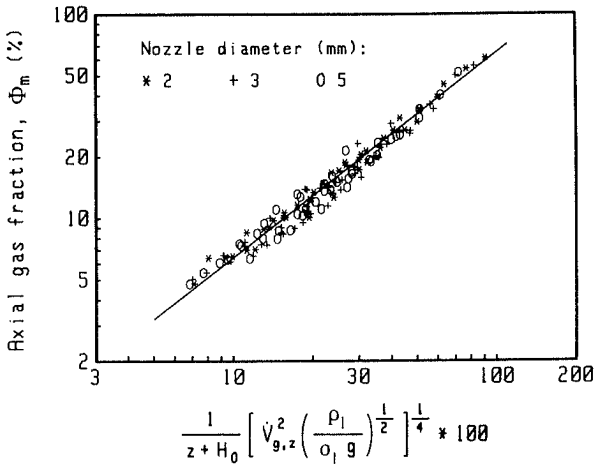

Fig. 6. Dimensionless description of the axial gas fraction.

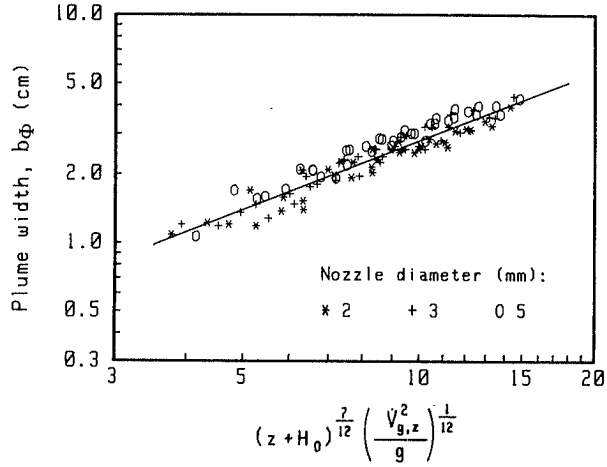

Fig. 7. Dependence of plume width on gas flow rate and height.

dimensional analysis the following expression for Φ_m was obtained:

$$\Phi_m = 0.65[\dot{V}_{g,z}^2(\rho_l/\sigma_l g)^{1/2}]^{1/4}/(z+H_0) \; . \quad .....(5)$$

Figure 6 shows the graphical plotting of the equation. For comparison the measured values of Φ_m are entered in the image. A good adaptation appears.

The bubble plume broadens with increasing distance from the nozzle and its width becomes larger with growing gas flow rate. The values of b_Φ obtained from the presented measurements result in the following relation:

$$b_\Phi = 0.28(z+H_o)^{7/12}(\dot{V}_{g,z}^2/g)^{1/12} \; . \quad .....(6)$$

As it is shown in **Fig. 7**, the values of b_Φ can be well described by this equation. It was also observed that the bubble plume shows an over-proportional broadening in the highest plane at $z=35$ cm. This is caused by the turn of liquid flow from the vertical to the radial direction in the region near the bath surface.

By the gas stirring treatment in ladle the inert gas is frequently blown through a porous plug which is located eccentrically in the bottom. Because of the asymmetric flow field the behaviour of the bubble plume is different from that at centric blowing. **Figure 8** represents as an example the distribution of gas fraction in the main vertical plane being spread through the eccentric nozzle and the center of the vessel for a gas flow rate of 500 Ncm^3/sec. As can be seen, the bubble plume obviously inclines to the wall. The reason for that is the different flow velocity of the surrounding liquid. If the liquid on one side of the bubble plume flows with a higher velocity, it will exert a traction on the bubble plume on this side. The bubble plume then displaces to this direction.

The phenomenon that effects a lateral deflection of the bubble plume during eccentric blowing should be taken into consideration for the positioning of the porous plug. If the plug is attached with a too great eccentricity in the bottom of the ladle, the gas bubbles will rise near the vessel wall. This could cause a strong local corrosion of the refractory material and possibly a deterioration of the metallurgical processes in the ladle.

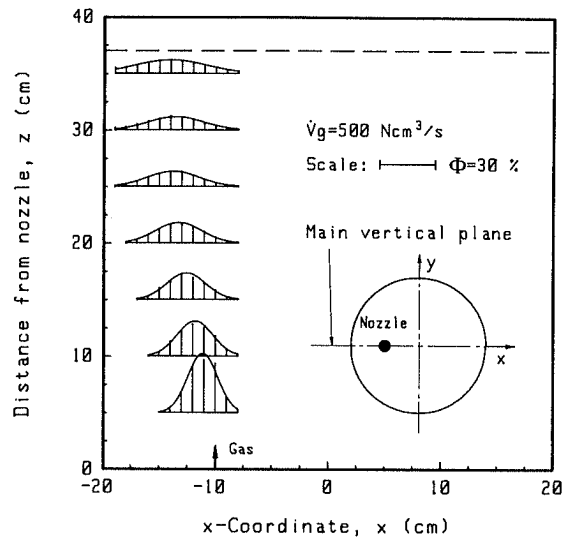

Fig. 8. Gas fraction profiles in the main vertical plane in case of eccentric blowing.

Despite the stable lateral deflection mentioned the distribution of gas fraction in the main plane during eccentric blowing also obeys a Gaussian function that in this case is modified as follows:

$$\Phi_{ecc,x} = \Phi_m \exp[-(x-x_m)^2/b_{\Phi,x}^2] \; . \quad .....(7)$$

Here x_m marks the x-coordinate of the plume center and $b_{\Phi,x}$ describes the width of the bubble plume in x-direction.

In **Fig. 9** the distributions of gas fraction for various y-coordinates, namely in various distances from the main plane for a gas flow rate of 200 Ncm^3/sec and at a height of 20 cm above the nozzle are presented. They can be described with the Gaussian function as well. The peaks of all curves lie at the same x-coordinate. The greatest gas fraction Φ_m occurs in the plane $y=0$ cm. The bubble plume is therefore specular symmetric about the main plane. Moreover, the measured data show that the distribution of gas fraction in y-direction at an x-coordinate of x_m can be expressed as follows:

$$\Phi_{ecc,y} = \Phi_m \exp(-y^2/b_{\Phi,y}^2) \; . \quad .....(8)$$

A comparison of the $b_{\Phi,x}$ value with the $b_{\Phi,y}$ value

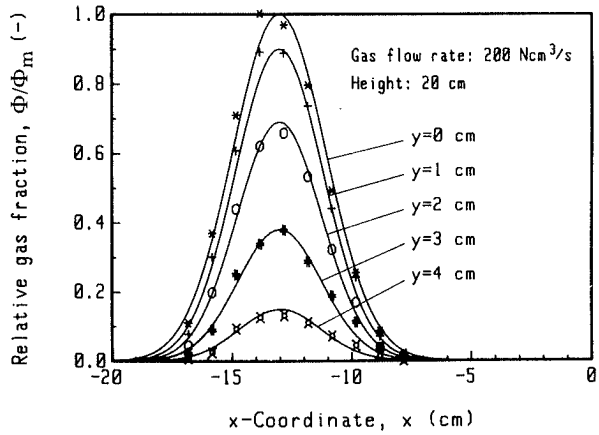

Fig. 9. Gas fraction distribution for various y-coordinates in case of eccentric blowing.

points out that the bubble plume in y-direction broadens more strongly than in x-direction. The ratio $b_{\Phi,x}/b_{\Phi,y}$ neither depends on the gas flow rate nor on the distance above the nozzle. In average the value of $b_{\Phi,y}$ is by 17% greater than that of $b_{\Phi,x}$. This means that the bubble plume in a horizontal plane in case of eccentric blowing has the shape of an ellipse, whereas it is circular at centric blowing.

From the measurements of local gas fraction the mean velocity of the gas stream in a cross section of the bubble plume can be determined. It results from the gas flow rate divided by the integral of the local gas fraction in a horizontal plane:

$$u_g = \dot{V}_g \left(\int_A \Phi dA \right)^{-1} . \quad \text{.....(9)}$$

For centric blowing the integral is:

$$\left(\int_A \Phi dA \right)_{cen} = \int_0^\infty 2\pi r \Phi dr . \quad \text{.....(10)}$$

If the local gas fraction Φ is inserted by Eq. (1), it will follow:

$$\left(\int_A \Phi dA \right)_{cen} = \int_0^\infty 2\pi r \Phi_m \exp\left(-\frac{r^2}{b_\Phi^2} \right) dr = \pi \Phi_m b_\Phi^2 , \quad \text{.....(11)}$$

To the eccentric blowing it applies:

$$\left(\int_A \Phi dA \right)_{ecc} = \Phi_m \int_{-\infty}^{\infty} \exp\left(-\frac{x^2}{b_{\Phi,x}^2} \right) dx \times \int_{-\infty}^{\infty} \exp\left(-\frac{y^2}{b_{\Phi,y}^2} \right) dy = \pi \Phi_m b_{\Phi,x} b_{\Phi,y} . \quad \text{.....(12)}$$

In **Fig. 10** the results calculated by Eqs. (11) and (12) are given. With the exception of the lowest plane $z=5$ cm there is no perceptible difference of the integral between centric and eccentric gas blowing. From this analysis it can be concluded that the nozzle position has no influence on the mean rising velocity of bubbles.

3.2. Bubble Frequency Distribution

The bubble frequency distribution was determined for different gas flow rates and nozzle diameters at

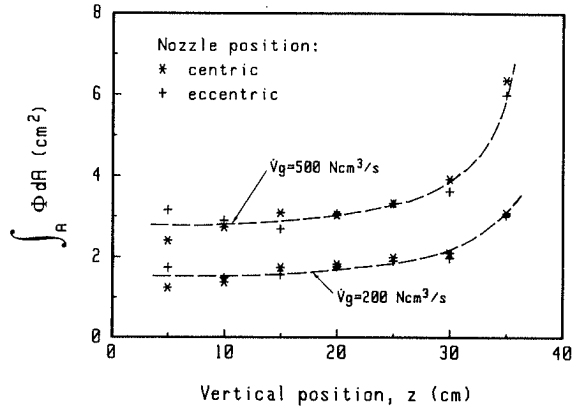

Fig. 10. Comparison between the integrations of gas fraction at centric and eccentric gas blowing.

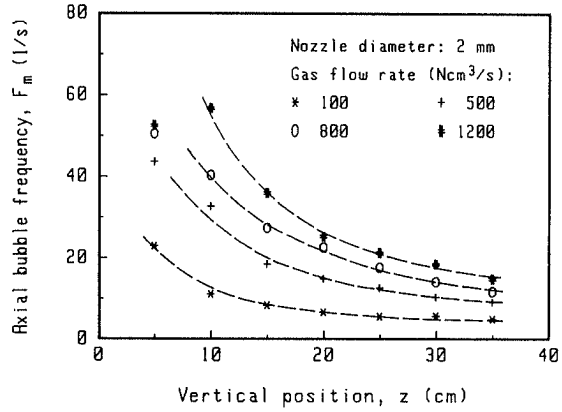

Fig. 11. Axial bubble frequency as a function of height and gas flow rate.

centric blowing. In analogy to the gas fraction the radial distribution of the bubble frequency can be described with a Gaussian function:

$$F_b = F_m \exp(-r^2/b_F^2) , \quad \text{.....(13)}$$

in which F_b marks the local bubble frequency, F_m the maximum and b_F an exponential factor of the distribution.

Like parameter b_Φ, b_F also describes the bubble plume width. It was found from the accomplished measurements that the difference between b_F and b_Φ is slight. The ratio of b_F/b_Φ generally lies in the range of 1 ± 0.05. Therefore Eq. (6) can also be employed for the determination of the b_F value.

The bubble frequency in the plume center increases with growing gas flow rate. For small gas flow rates its vertical alteration over the total height follows an exponential function. Different from that, curves for large gas flow rates can only be described by an exponential function from a height of about 10 cm on, as it is presented in **Fig. 11**. Below this level the measured values show a negative deviation from the curves. The reason for that is obviously that with increasing gas flow rate the bubbles formed at the nozzle become larger. In this way the bubble frequency within the region close to the nozzle is not proportional to the gas flow rate. The thus revealed influence of gas flow rate diminishes by break-up of the large bubbles

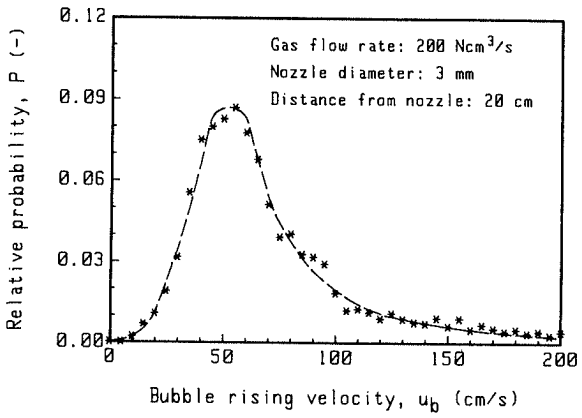

Fig. 12. Distribution of bubble rising velocity.

during their rising and vanishes at about 10 cm above the nozzle.

With the assistance of a regression analysis the following numerical equation is established:

$$F_m = 11.46 \dot{V}_{g,z}^{0.55}/(z+H_o)\,, \quad \text{.....(14)}$$

where $\dot{V}_{g,z}$ is specified in cm³/sec, z and H_o in cm. The lined curves in Fig. 11 correspond to this relation. Owing to the deviation at the lowest plane $z=5$ cm the equation is valid for $z \geq 10$ cm.

3.3. Rising Velocity of Bubbles

The rising velocity of gas bubbles in the molten metal was investigated under different blowing conditions. The measurements show that the single bubbles in the plume rise with very different velocity. **Figure 12** represents as an example the relative probability distribution of the bubble rising velocity at a gas flow rate of 200 Ncm³/sec and a height of 20 cm above the nozzle. An asymmetrical distribution with a steep flank on the left and a flat one on the right with a pronounced maximum at about 55 cm/sec is yielded. The values of the bubble rising velocity lie within the range of 10 to 200 cm/sec. Such a wide velocity spectrum may be caused by a turbulent fluid flow in the bubble plume and by a wide bubble size distribution.

In order to estimate the mean rising velocity of bubbles, an arithmetic average value of the velocity spectrum is formed according to:

$$\bar{u}_b = \frac{1}{N}\sum_{i=1}^{N} u_b(i)\,, \quad \text{.....(15)}$$

N is the number of measured bubbles. However, it has to be pointed out that this average value must not represent accurately the mean velocity of the gas stream, because the volumes of bubbles with different sizes are not considered in the calculation. If large bubbles rise with a higher velocity in the plume, a lower average value will be represented by this equation than the actual mean velocity of the gas.

Figure 13 shows the radial alteration of the average velocity formed by Eq. (15) at a gas flow rate of 200 Ncm³/sec in different planes. In the lowest plane $z=5$ cm a maximum in the plume center can be perceived. With increasing distance from the nozzle the

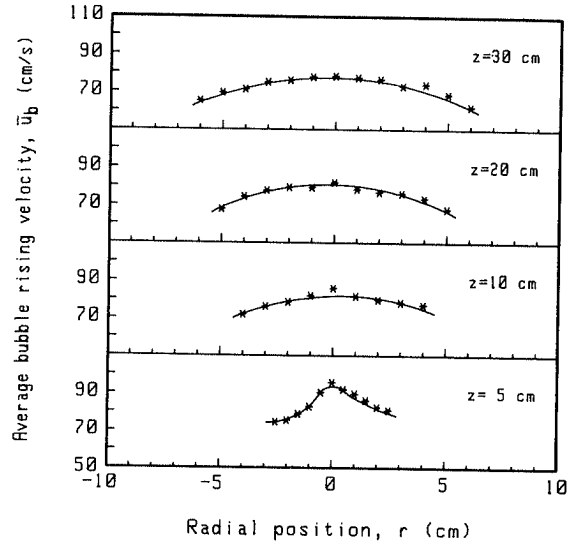

Fig. 13. Profiles of average bubble rising velocity in various cross sections of the plume at a gas flow rate of 200 Ncm³/sec.

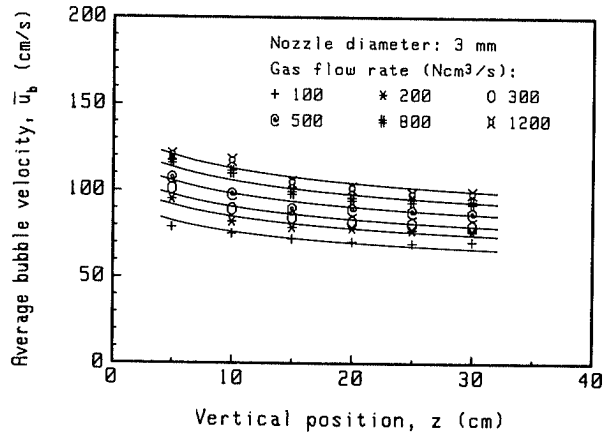

Fig. 14. Vertical alteration of average bubble rising velocity.

average values equalize more and more in radial direction. Except for the region near the nozzle the bubble rising velocity over the radius is thus almost constant.

As represented above, the mean velocity of gas stream in the bubble plume can be established from the measurements of local gas fraction. By means of Eqs. (5), (6), (9) and (11) one obtains the following expression for u_g:

$$u_g = 75.73[\dot{V}_{g,z}/(z+H_o)]^{1/6}\,. \quad \text{.....(16)}$$

Here u_g is given in cm/sec, $\dot{V}_{g,z}$ in cm³/sec, z and H_o in cm.

According to the only slight alteration of the bubble rising velocity in radial direction, an average value is formed of all measured bubbles in a horizontal plane for the investigation of the vertical change of bubble rising velocity. As **Fig. 14** points out, the average value gradually increases with growing gas flow rate. Its vertical alteration is slight. It was found that the dependence of $\bar{u}_b$ from the gas flow rate and the vertical position is the same as that of u_g. However, for the description of $\bar{u}_b$ a factor of 54.51 instead of 75.73 in Eq. (16) has to be employed. The curves in Fig. 14 represent

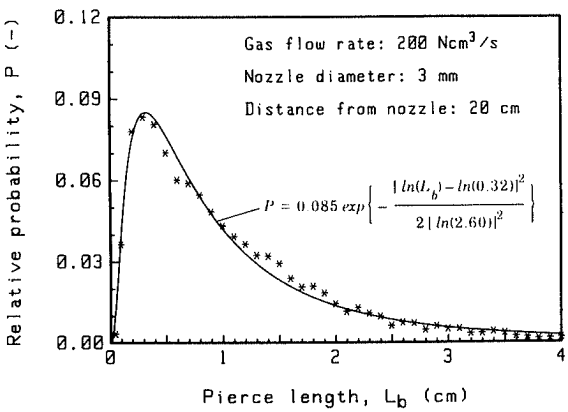

Fig. 15. Distribution of bubble pierce length.

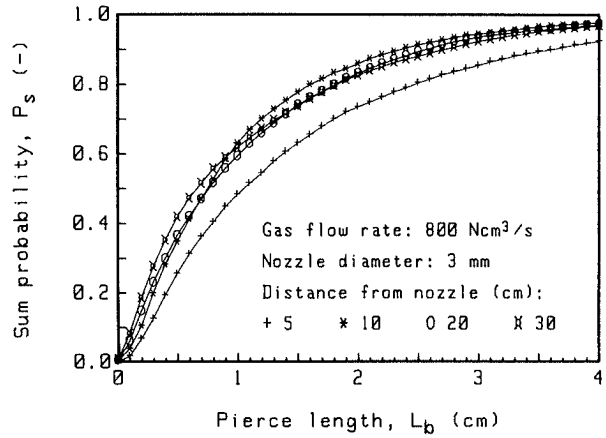

Fig. 16. Sum probability distribution of bubble pierce length at various heights.

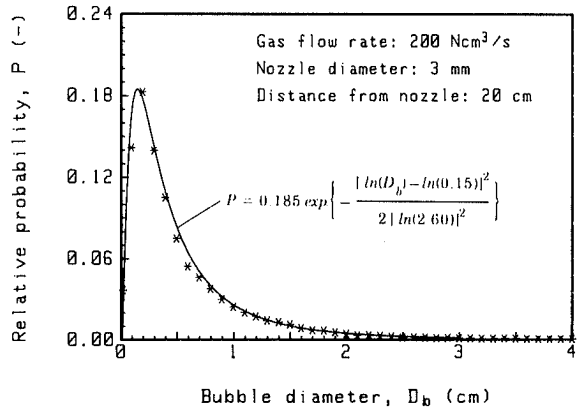

Fig. 17. Distribution of bubble diameter calculated with the Spector-method.

this dependence. The fact that the factors for u_g and $\bar{u}_b$ are different indicates that the rising velocity of bubbles in the plume depends on their size. Large bubbles rise with a higher velocity.

3.4. Bubble Size

Because the bubbles are not always pierced in their center by the double-contact electroresistivity probe, not the diameter but the pierce length of bubbles is measured. The single measurement of the pierce length cannot be referred to the bubble size. However, it is possible from a great number of single measurements to make qualitative statements about the bubble size. Besides, the bubble size distribution can be calculated with a statistic evaluation procedure from the spectrum of the pierce length.

In **Fig. 15** an example of the measured distribution of the pierce lengths is to be seen. The spectrum after a primarily steep ascent of the curve shows a distinct maximum of the relative probability in the range of 2 to 4 mm and then slowly falls down. The largest pierce length amounts to about 40 mm.

The spectrum of the pierce length can be described by a logarithmic normal function in the form of

$$P = P_m \exp\{-[\ln(x) - \ln(x')]^2 / 2[\ln(s)]^2\}\ , \quad \text{.....(17)}$$

where P_m shows the maximum relative probability, x' the x-coordinate of the maximum and s the standard deviation of the distribution. The curve in Fig. 15 shows the distribution calculated according to this equation with a value of $s = 2.6$ cm. The adaptation of the curve to the measured data is satisfying.

The radial alteration of the pierce length was investigated as well. It was found that the distribution of the pierce length in radial direction does not exhibit a perceptible difference. That means that the radial alteration of the bubble size is small. In the following explanations the pierce length and the bubble size are therefore considered to be independent from the position in radial direction.

Figure 16 shows the distributions of the pierce length at various heights above the nozzle for a gas flow rate of 800 Ncm^3/sec. In order to make it clear, they are represented in the form of a sum probability. As it is seen, the curve for the plane of 5 cm above the nozzle lies plainly below those for the planes of 10 cm and higher. It signifies that the bubbles are larger in the region near the nozzle than in the fully developped bubble plume. The distributions for all higher planes fall together. The remaining differences are scatter. The same was observed for the other gas flow rates.

From the pierce length distribution the bubble size can only qualitatively be estimated, but no quantitative statements can be made about the bubble size distribution and the average bubble diameter. In order to determine the bubble size distribution from the spectrum of the pierce length, the Spektor-method[11] was employed. **Figure 17** demonstrates the bubble size distribution calculated from the pierce length distribution shown in Fig. 15. Its functional description confirms the statement of earlier measurements in the system water/air[2,4] that the bubble size distribution follows a logarithmic normal function.

Beside the bubble size distribution, the knowledge of the number of bubbles is also needed for calculation of the gas/liquid interface. For single bubble classes this affords some recalculation. For simplicity, the calculation takes place here with the mean bubble size and the steady-state gas volume in the bath. The steady-state gas volume can be determined by the measurement of the local gas fraction:

$$V_g = \int_0^H \left(\int_A \Phi dA \right) dz\ . \quad \text{.....(18)}$$

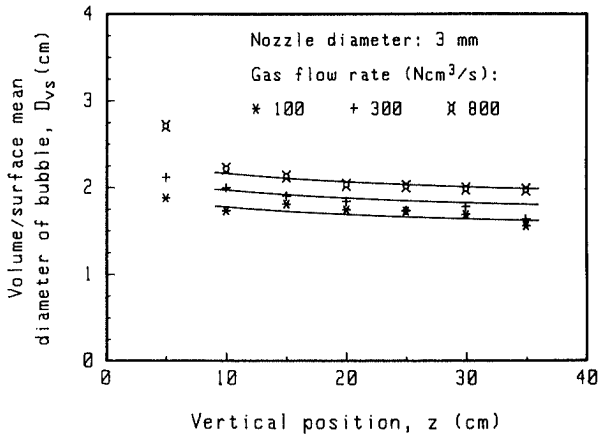

Fig. 18. Volume/surface mean bubble diameter for various gas flow rates and heights.

From the bubble size distribution a mean value can be formed according to different definitions. For processes of mass and heat transfer it is however expedient to form the volume/surface equivalent diameter as a mean value of the spectrum. This diameter is defined as follows:

$$D_{vs} \equiv \frac{\sum_i N_b(i) d_b^3(i)}{\sum_i N_b(i) d_b^2(i)} = \frac{\sum_i P(i) d_b^3(i)}{\sum_i P(i) d_b^2(i)}, \quad \text{.....(19)}$$

where $N_b(i)$ is the number, $d_b(i)$ the diameter and $P(i)$ the relative probability of bubbles within the class i.

From the results it was found that the nozzle diameter has no influence on the bubble size. With growing gas flow rate the bubble size in front of the nozzle distinctly increases. With increasing distance from the nozzle the influence of the gas flow rate becomes smaller due to the break-up of large bubbles. At a given gas flow rate the bubble size from a height of about 10 cm above the nozzle on changes only little. Except for the region close to the nozzle, the following dependence of the mean diameter from the gas flow rate and the height is obtained:

$$D_{vs} = 1.46[\dot{V}_{g,z}/(z+H_o)]^{0.1}, \quad \text{.....(20)}$$

in which $\dot{V}_{g,z}$ is given in cm³/sec, D_{vs}, z and H_o in cm.

In **Fig. 18** the mean diameters for three gas flow rates of 100, 300 and 800 Ncm³/sec are presented. The extremely slight alteration characterizes the establishment of a steady state for the bubble size distribution. In this state the bubble size is almost independent from the blowing conditions. The processes of the bubble break-up and coalescence are obviously in a dynamic equilibrium.

3.5. Influence of Gas Properties

In order to determine the influence of the physical properties of gas on the bubble behaviour, the distribution of gas fraction and bubble frequency as well as the bubble rising velocity and the bubble size were also measured in the case of blowing with argon and helium at a gas flow rate of 200 Ncm³/sec. For all these variables no observable difference between blowing with nitrogen, argon or helium was found. Hence the gas properties have no influence on the bubble behaviour.

4. Discussion

4.1. Mathematical Description of Gas Fraction

The gas fraction distribution is let to be characterized by the parameters Φ_m and b_Φ. Instead of b_Φ, the characteristic magnitude of the bubble plume width is also often indicated with the half-value radius $r_{1/2}$, the gas fraction here amounting to half of Φ_m. Between b_Φ and $r_{1/2}$ the following relation exists:

$$b_\Phi = 1.20 r_{1/2}. \quad \text{.....(21)}$$

In earlier papers[1,4,5,7] both parameters have been described as functions of the dimensionless height z/d_o and the Froude number at the nozzle position that is modified by the densities of liquid and gas. Thus, the following equations for instance were set up in the paper of Tacke *et al.*,[1]

$$\Phi_m = 50\left\{0.20\frac{z}{d_o}\left[\frac{g d_o^5 \rho_l}{\dot{V}_g^2 \rho_g}\right]^{0.33}\right\}^{-\gamma}, \quad \text{.....(22)}$$

$$r_{1/2}\left(\frac{g}{\dot{V}_g^2}\right)^{1/5} = 0.42\left\{0.20\frac{z}{d_o}\left[\frac{g d_o^5 \rho_l}{\dot{V}_g^2 \rho_g}\right]^{0.30}\right\}^{\beta}. \quad \text{...(23)}$$

For γ and β the values of 1.22 and 0.78 for the system air/water, and the values of 0.866 and 0.56 for the systems nitrogen/mercury and helium/water were given. According to these equations the gas fraction in the plume center and the plume width strongly depend on the nozzle diameter and on the gas density. The measurements performed in the present paper show however that the nozzle diameter has an only slight influence on the distribution of gas fraction and that the gas density does not matter at all. Moreover, it is unsatisfying that the exponents in Eqs. (22) and (23) are still different for various systems, when the densities of liquid and gas as influencing parameters are already considered in the equations.

As the gas fraction in the bubble plume is coupled with the bubble rising velocity, the physical properties of liquid, such as the density and the surface tension of liquid, which have an influence on the bubble rising velocity should be considered. According to this viewpoint the quotient $(\rho_l/\sigma_l g)$ was entered into Eq. (5). It is to be expected that the data obtained in other systems can also be described with the relations developed here. In **Figs. 19** and **20** the Φ_m and b_Φ values of Tacke *et al.*[1] and of Zhou[5] are represented for the systems water/air and mercury/nitrogen according to the Eqs. (5) and (6). For comparison the straight lines obtained from the appropriate results for the system Wood's metal/nitrogen are also entered. Although the densities and the surface tensions of water, mercury and Wood's metal are very different, the data at all three systems can be described with one respective equation. It is true that the data of Tacke *et al.* in the water model show a relatively great deviation, but still let to find a linear dependence.

Moreover, it was observed that for the system

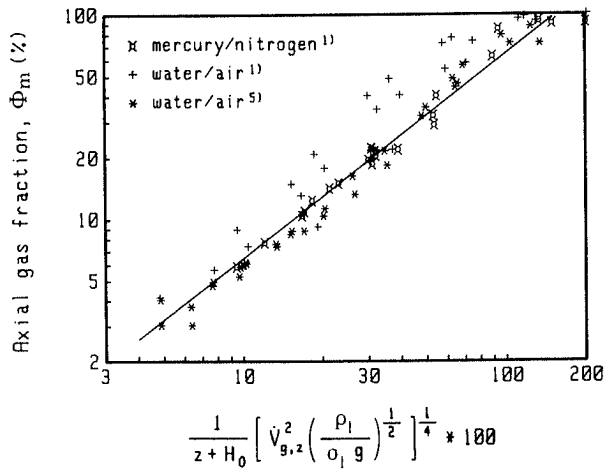

Fig. 19. Comparison of axial gas fraction in different systems.

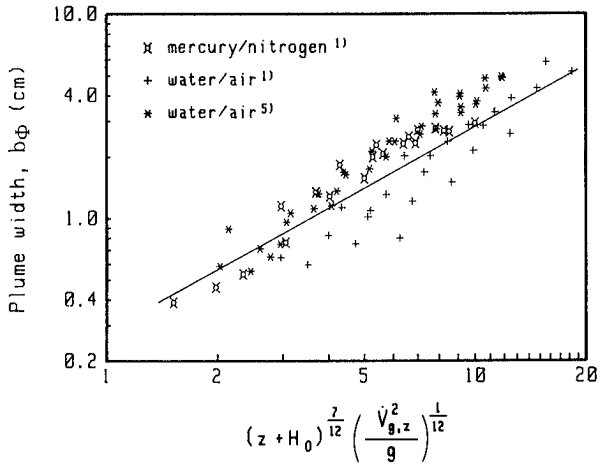

Fig. 20. Comparison of plume width in different systems.

water/air smaller values of H_o should be used than those calculated with Eq. (4), in order to get a better linear dependence. This can be explained such that the penetration depth of the gas jet is larger in the water bath and the bubble plume in the region close to the nozzle broadens less strongly than in molten metals. According to Engh *et al.*[12] the penetration depth of a gas jet in a liquid is inversely proportional to the liquid density with an exponent of 1/3. for this reason the H_o value depends on the liquid density. For the representation of the data at systems mercury/nitrogen and water/air a value of $4.5(\rho_l/\rho_{wood})^{1/3}$ was employed for the constant in Eq. (4).

4.2. Relation between Bubble Frequency and Bubble Size

The distribution of the bubble frequency is connected with the bubble size. At a constant gas flow rate the bubble frequency is all the smaller, the larger the bubbles are. Irrespective of the bubble shape it can be supposed that the projection area of the bubbles is circular. With this assumption the number of bubbles per unit of time passing a cross section of the plume may be expressed by

$$\dot{N}_b=\frac{1}{\pi r_b^2}\int_0^\infty 2\pi r F_b dr=F_m b_F^2/r_b^2\,, \quad \text{.....(24)}$$

r_b here marks the average radius of bubbles. On the other hand the number of bubbles can be calculated according to the gas volume balance:

$$\dot{N}_b=\dot{V}_{g,z}/(4\pi r_b^2/3)\,. \quad \text{.....(25)}$$

From the combination of Eqs. (24) and (25) it results:

$$r_b=3\dot{V}_{g,z}/4\pi F_m b_F^2\,. \quad \text{.....(26)}$$

This equation is derived from the assumption that the bubbles are spherical. For ellipsoidal bubbles with a radius ratio of b/a (short radius/long radius) the volume amounts to $4\pi a^2 b/3$ and the projection area to πa^2. If these two expressions are inserted into Eqs. (24) and (25) respectively, the same expression as Eq. (26) will result. Hence, Eq. (26) is also valid for ellipsoidal bubbles. However in this case r_b marks the short radius of bubbles.

Inserting Eq. (6) with $b_F=b_\Phi$ and Eq. (13) into Eq. (26), one obtains the following numerical relation:

$$r_b=0.60\dot{V}_{g,z}^{0.117}/(z+H_o)^{1/6}\,, \quad \text{.....(27)}$$

in which $\dot{V}_{g,z}$ is given in cm^3/sec, r_b, z and H_o in cm. It corresponds well with Eq. (20). Also in this equation an insignificant influence of the gas flow rate on the bubble size is shown.

4.3. Influence of Bubble Shape on Mean Diameter D_{vs}

Equation (20) gives the volume/surface mean diameter for spherical bubbles. According to the bubble size distribution most of the bubbles have a diameter of 2 to 15 mm. Bubbles within this magnitude have an ellipsoidal shape. For non-spherical bubbles the volume/surface mean diameter can be determined as follows:

$$D_{vs}=6\sum_i P(i)V_b(i)/\sum_i P(i)A_b(i), \quad \text{.....(28)}$$

here $V_b(i)$ means the volume and $A_b(i)$ the surface of bubbles within the class i.

The shape of ellipsoidal bubbles is characterized by their short radius b and long radius a. The smaller the radius ratio b/a is, the more flat the bubbles are. Calculations with different radius ratios show that the D_{vs} value increases with decreasing b/a value for a given distribution of the short radius of bubbles. That can be explained by the following execution.

For spherical bubbles one has:

$$V_b(i)/A_b(i)=[4\pi r_b^3(i)/3]/4\pi r_b^2(i)=r_b(i)/3\,. \quad \text{....(29)}$$

For ellipsoidal bubbles the volume amounts to:

$$V_b(i)=4\pi a^2(i)b(i)/3 \quad \text{.....(30)}$$

and the surface[13]:

$$A_b(i)=2\pi a(i)b(i)\left\{\frac{a(i)}{b(i)}+\ln\left[\frac{a(i)}{b(i)}+\left(\frac{a^2(i)}{b^2(i)}-1\right)^{1/2}\right]\times\left(\frac{a^2(i)}{b^2(i)}-1\right)^{-1/2}\right\}. \quad \text{.....(31)}$$

The ratio of the volume to the surface is:

$$V_b(i)/A_b(i)=2b(i)/3(1+K)\,, \quad \text{.....(32)}$$

with

$$K=\frac{b(i)}{a(i)}\ln\left[\frac{a(i)}{b(i)}+\left(\frac{a^2(i)}{b^2(i)}-1\right)^{1/2}\right]\left(\frac{a^2(i)}{b^2(i)}-1\right)^{-1/2}$$

For $b(i)/a(i)<1$, K is always smaller than one. With decreasing $b(i)/a(i)$ value K becomes smaller and the ratio $V_b(i)/A_b(i)$ however larger which leads to a great D_{vs} value. For $b(i)/a(i)=1$, namely for spherical bubbles, K reaches the maximum one. Equation (32) then changes into Eq. (29).

With the help of Eq. (32) the influence of the bubble shape on the volume/surface mean diameter can be estimated. It was found that this influence is not very large. Hence, it can be concluded that the assumption of spherical bubbles has no aggravating mistake for the evaluation to follow.

5. Conclusions

In this paper the local gas fraction, the bubble frequency, the bubble size and the bubble rising velocity at gas blowing into molten Wood's metal in a ladle shaped vessel were experimentally determined. From the measurements the following can be concluded:

(1) At gas blowing through a single nozzle positioned centrically as well as eccentrically, the distribution of the gas fraction and of the bubble frequency in a horizontal plane can be described with a Gaussian function. At centrical blowing the bubble plume is axisymmetric and its cross section is circular. In distinction from that the bubble plume at eccentrical blowing is symmetric about the main plane in which the eccentric nozzle and the vessel axis are located. The bubble plume has an elliptic cross section and inclines to the vessel wall. The characteristic parameters of the distribution of gas fraction and of bubble frequency predominantly depend on the gas flow rate and on the distance from the nozzle. The nozzle diameter has a small influence only in the region close to the nozzle.

(2) Gas bubbles in the plume rise with very different velocities. A velocity spectrum occurs. Except for the nozzle region the average velocity in radial direction is nearly constant. The mean bubble rising velocity increases with growing gas flow rate and its vertical alteration is not considerable. The nozzle position has no influence on it.

(3) The bubble size in the plume is determined by break-up and coalescence processes. In the region close to the nozzle the process of break-up predominates. From a height of about 10 cm on above the nozzle the bubble size distribution alters very little. The bubble size distribution follows a logarithmic normal function and alters very little from a height of about 10 cm on above the nozzle.

(4) The physical properties of the injected gas have no perceptible influence on the bubble behaviour.

Acknowledgement

This research work was financially supported by Deutsche Forschungsgemeinschaft, which is gratefully acknowledged.

Nomenclature

a: Long radius of ellipsoidal bubbles (cm)
A: Area (cm^2)
b: Short radius of ellipsoidal bubbles (cm)
b_F, b_Φ: Plume width with reference to bubble frequency and gas fraction respectively (cm)
d_o: Nozzle diameter (cm)
D_{vs}: Volume/surface mean diameter (cm)
F_b: Local bubble frequency (1/sec)
F_m: Axial bubble frequency (1/sec)
g: Acceleration of gravity (cm/sec^2)
H: Bath height (cm)
L_b: Bubble pierce length (cm)
N: Number of bubbles
p_N: Standard pressure (g/cm·sec^2)
P: Relative probability
P_s: Sum probability
r: Radial position (cm)
r_b: Radius of bubble (cm)
$r_{1/2}$: Half-value radius (cm)
T_l: Temperature of liquid (K)
T_N: Standard temperature (K)
u_b: Bubble rising velocity (cm/sec)
u_g: Gas velocity (cm/sec)
V: Volume (cm^3)
$\dot{V}_g$: Gas flow rate (cm^3/sec)
x, y, z: Coordinates (cm)
ρ_l: Liquid density (g/cm^3)
σ_l: Surface tension of liquid (g/sec^2)
Φ: Local gas fraction
Φ_m: Axial gas fraction

Subscripts
cen: Centric gas blowing
ecc: Eccentric gas blowing

REFERENCES

1) K. H. Tacke, H. G. Schubert, D. J. Weber and K. Schwerdtfeger: *Metall. Trans. B*, **16B** (1985), 263.
2) M. Kawakami, Y. Kitazawa, T. Nakamura, T. Miyake and K. Ito: *Trans. Iron Steel Inst. Jpn.*, **25** (1985), 394.
3) M. Sano, H. Makino, Y. Ozawa and K. Mori: *Trans. Iron Steel Inst. Jpn.*, **26**, (1986), 298.
4) A. H. Castillejos and J. K. Brimacombe: Scaninjective IV, 4th Int. Conf. on Injection Metallurgy, Luleå, Sweden, (1986).
5) M. Zhou: Ph. D. Thesis to Central Iron and Steel Research Institute, Beijing, China, (1988).
6) M. A. S. C. Casstello-Branco and K. Schwerdtfeger: 26th Annual Conf. of Metallurgists, Winnipeg, (1987).
7) S. C. Koria and S. Singh: *Steel Res.*, **60** (1989), 301.
8) M. Iguchi, H. Takeuchi and Z. Morita: *Trans. Iron Steel Inst. Jpn.*, **31** (1991), 246
9) J. C. Ralph: *The Chemical Engineer*, **11** (1973), 512.
10) S. H. Chung and K. W. Lange: *Steel Res.*, **60**, (1989), 49.
11) E. E. Underwood: Particle-size Distribution, ed. by T. D. Robert and N. R. Frederick, McGraw-Hill, New York, (1968), 149.
12) T. A. Engh, K. Larsen and K. Venas: *Ironmaking Steelmaking*, **6** (1979), 268.
13) Y. Xie: Ph. D. Thesis to Berlin Technical University, Berlin, (1991).